PAPER

Charge transfer in $(PbSe)_{1+\delta}$ $(NbSe_2)_2$ and $(SnSe)_{1+\delta}$ $(NbSe_2)_2$ ferecrystals investigated by photoelectron spectroscopy

To cite this article: Fabian Göhler et al 2018 J. Phys.: Condens. Matter 30 055001

View the article online for updates and enhancements.

Related content

- Heterostructures containing dichalcogenides-new materials with predictable nanoarchitectures and novel emergent properties Danielle M Hamann, Erik C Hadland and David C Johnson
- <u>Ferecrystals: non-epitaxial layered intergrowths</u>
 Matt Beekman, Colby L Heideman and David C Johnson
- <u>Synthesis and characterization of turbostratically disordered</u>
 (BiSe) 1.15TiSe 2
 Devin R Merrill, Daniel B Moore, Mark N
 Coffey et al.



IOP ebooks™

Bringing you innovative digital publishing with leading voices to create your essential collection of books in STEM research.

Start exploring the collection - download the first chapter of every title for free.

Charge transfer in $(PbSe)_{1+\delta}(NbSe_2)_2$ and $(SnSe)_{1+\delta}(NbSe_2)_2$ ferecrystals investigated by photoelectron spectroscopy

Fabian Göhler¹, Gavin Mitchson², Matti B Alemayehu², Florian Speck¹, Martina Wanke¹, David C Johnson² and Thomas Seyller¹

- ¹ Institut für Physik, Technische Universität Chemnitz, Reichenhainer Straße 70, D-09126 Chemnitz, Germany
- ² Department of Chemistry, University of Oregon, Eugene, OR 97401, United States of America

E-mail: thomas.seyller@physik.tu-chemnitz.de

Received 20 October 2017, revised 27 November 2017 Accepted for publication 15 December 2017 Published 5 January 2018



Abstract

Rotationally disordered, layered (PbSe) $_{1+\delta}(NbSe_2)_2$ and (SnSe) $_{1+\delta}(NbSe_2)_2$ ferecrystal heterostructures, consisting of stacked two-dimensional bilayers of either PbSe or SnSe alternating with two planes of NbSe $_2$, were synthesized from modulated elemental reactants. The electronic structure of these ternary systems was investigated using x-ray photoelectron spectroscopy and compared to the binary bulk compounds PbSe, SnSe and NbSe $_2$. The Pb and Sn core level spectra show a significant shift towards lower binding energies and the peak shape becomes asymmetric in the ferecrystals, while the electronic structure of the NbSe $_2$ layers does not change compared to the bulk. This is interpreted in terms of an interlayer interaction in the form of a charge transfer of electrons from PbSe or SnSe into the NbSe $_2$ layers, which is supported by valence band spectra and is consistent with prior results from transport measurements.

Keywords: ferecrystals, van-der-Waals materials, charge transfer, layered heterostructures, transition metal dichalcogenides

(Some figures may appear in colour only in the online journal)

1. Introduction

Two-dimensional materials have been in the focus of the scientific community ever since the groundbreaking work on graphene by Novoselov and Geim [1]. In recent years, the stacking of two dimensional sheets into so-called van-der-Waals heterostructures has become an emerging field, and is a powerful concept to create new materials [2–8]. Researchers have discovered that properties can be controlled by controlling nanoarchitecture. The layering sequence, layer thicknesses, choice of constituents, and substrate all can be used to tune both structure and properties [9]. For example, graphene films on hexagonal boron nitride substrates have much larger carrier mobility than when they are on silicon oxide substrates [10–12]. FeSe monolayer films deposited on strontium titanate have enhanced superconducting critical temperatures due to charge transfer from the substrate [13], and borophene

monolayers on a silver substrate exhibited metallic behavior unique from the semiconducting behavior of other boron-based allotropes [9]. The designed self-assembly of van-der-Waals heterostructures from amorphous modulated precursors has recently been demonstrated for VSe₂—GeSe₂ heterostructures [14]. The structures of rock salt-like 2D layers have also been found to vary systematically with thickness and also with the dichalcogenide constituent they are layered with in heterostructures [15–17]. These van-der-Waals materials are synthesized from amorphous modulated precursors and have been termed ferecrystals due to their extensive turbostratic disorder [18]. Low-dimensional systems like these provide unique opportunities to put atoms in unusual bonding arrangements, resulting in optimized and/or emergent physical properties.

Ferecrystals consist of stacked two-dimensional layers of metal chalcogenides MX and transition metal dichalcogenides TX₂. Here, M is a metal of group 14 or 15 of the periodic

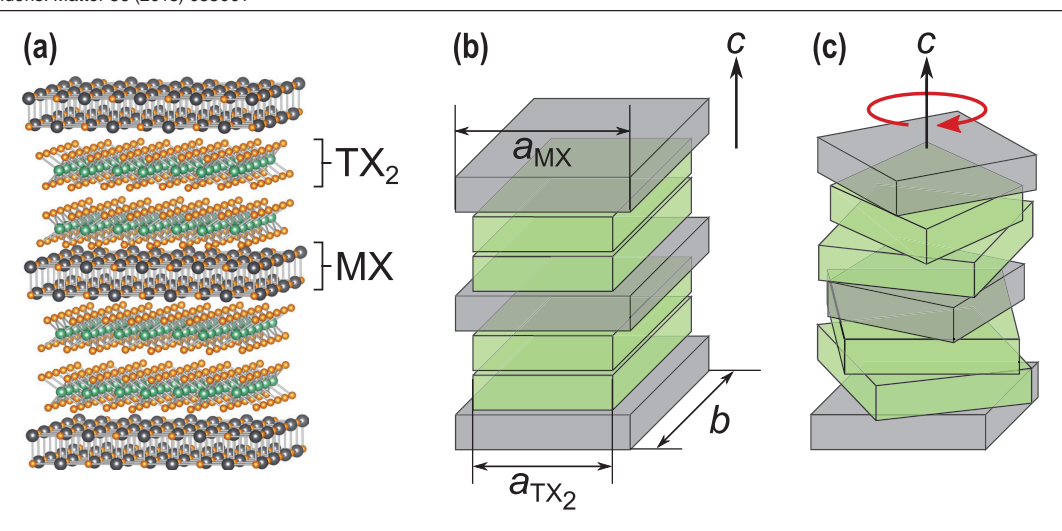


Figure 1. Layer structure and layer alignment of $[(MX)_{1+\delta}]_1(TX_2)_2$ heterostructures: (a) single layers of rocksalt-like MX alternate with two layers of TX_2 . (b) There is an epitaxial relationship between layers in conventional misfit layer compounds. (c) In ferecrystals, the layers show random rotational disorder along the c-axis ((b), (c) after [19]).

table (e.g. Pb, Sn or Bi), T is a transition metal (e.g. Ti, V, Nb, Ta etc.) and X is a chalcogen (either S, Se or Te). The general formula of ferecrystals is $[(MX)_{1+\delta}]_m(TX_2)_n$, where m and n are integers corresponding to the number of layers, and δ is the so-called misfit parameter due to the different lattice constants a_{MX} and a_{TX_2} (see figure 1) of the MX and TX₂ sublattices [18]. Individual layers show strong intralayer bonding and there are only weak interlayer interactions to hold the layers together. Both of the two sublattices retain a lot of structural features from the corresponding bulk materials. The MX layers show a distorted rocksalt structure, where the metal atoms M move out of plane with respect to the X atoms and closer to the neighboring TX₂ layers (which is generally called 'puckering'). In the TX2 layers, a layer of transition metal atoms is sandwiched between two layers of chalcogen atoms in either a trigonal-prismatic or octahedral coordination, depending mostly on the transition metal (figure 1(a)).

Ferecrystals are closely related to the class of misfit layered compounds (MLCs) [20, 21], but show some distinct structural differences and a much broader range of possible compositions due to their unique low-temperature self-assembled preparation (see section 2). In ferecrystal synthesis, the number of stacked individual layers m and n can be controlled independently, and values as large as 30 have been reported [16]. Products that are only kinetically stable, like the telluride ferecrystals [22] and those containing MoSe₂ and WSe₂ [23– 25], can be prepared as well as polymorphs of conventional MLCs and a virtually unlimited number of structural isomers [26]. While MLCs show an epitaxial relationship between the individual layers with a commensurate in-plane axis (labeled b in figure 1(b)) [20], in ferecrystals no such relationship exists and individual layers and individual grains show extensive rotational disorder along the c-axis of the crystal (figure 1(c)) [27]. This rotational (or turbostratic) disorder leads to significantly lowered cross-plane thermal conductivity which may be useful for thermoelectric applications [24, 25, 28]. Studies comparing ferecrystals to their epitaxial counterparts usually find differing physical properties [19, 29, 30].

With the structure of the layers in the heterosystem being close to the corresponding bulk material, it is expected that also the electronic structures remain largely conserved [18–21]. Thus, ferecrystals (as well as MLCs) are often described in the framework of a rigid band model, where the electronic structure (density of states) of the intergrowth is approximated by a superposition of the electronic structures of the MX and TX_2 components. The conduction is dominated by the TX_2 layers [31].

Changes in the electronic structures of the single components may then arise in the form of band filling due to charge transfer from one layer to another. Alemayehu et al [32-35] observed in their transport measurements that the electrical resistivity increases and the carrier concentration decreases in $[(MSe)_{1+\delta}]_m(NbSe_2)_n$ ferecrystals, where M is either Pb or Sn, if m is increased. They conclude that electron transfer occurs from the MSe layers to the NbSe2 layer, which reduces the carrier concentration in the NbSe2 layer. The charge carrier concentration increases if n is increased, supporting the idea that conduction is dominated by the dichalcogenide layers [36]. A proposed band alignment is shown in figure 2. If the Fermi energy $E_{\rm F}$ is lower in NbSe₂ than in PbSe, electrons can be transferred into the half-filled Nb4d band of NbSe₂ [32]. Studies on structural isomers show that there is a functional separation of the constituent layers, with MSe serving as a charge donating layer and NbSe₂ with its high mobility as a transport layer [37].

Charge transfer was also suggested as a potential reason for the stability of MLCs. As summarized by Wiegers [38], electrons are donated from the MX into the TX_2 layer in MLCs where M is a rare earth metal. However, there was some controversy if charge transfer also takes place, if one looks at MLCs where M is a divalent cation (Sn or Pb) and T = Ti, Nb or Ta. From photoelectron spectroscopy, Ettema *et al* [39, 40] concluded that little or no charge transfer occurs, but instead there is covalent interlayer bonding. Ohno [41, 42] reported evidence for charge transfer based on x-ray photoelectron spectroscopy (XPS) valence band spectra for (PbS)₁₊₆ TiS₂

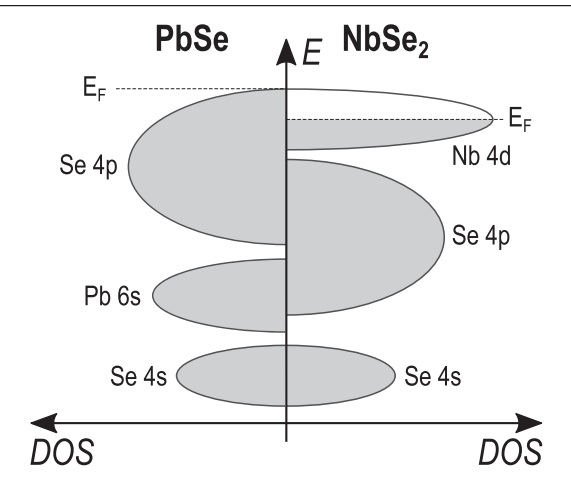


Figure 2. Schematic of expected band alignment that would allow charge transfer in (PbSe)_{1+ δ}(NbSe₂)₂: PbSe is a narrow band gap semiconductor while NbSe₂ is a p-type metal with a half filled d-band. In a heterostructure, electrons from the Se4p band of PbSe can fill empty states in the Nb4d band of NbSe₂ (after [32]).

and $(SnS)_{1+\delta}NbS_2$. Fang et al [43] concluded from photoelectron spectroscopy results and bandstructure calculations that there is a small charge transfer as well as covalent interlayer bonding in $(SnS)_{1+\delta}NbS_2$. In addition, Moëlo and Meerschaut et al [44, 45] claimed that interlayer charge transfer is the result of a T for M substitution in the MX layers based on investigations with electron probe microanalysis. Brandt et al [46] used angle resolved photoelectron spectroscopy (ARPES) to compare the misfit compound (PbS)_{1.14}NbS₂ to the layered dichalcogenide NbSe2 and found evidence for interlayer charge transfer, but they also see a difference in band dispersions and thus question the validity of a strict rigid band model. They followed up with an ARPES study that supported the occurrence of charge transfer in $(PbS)_{1.18}(TiS_2)_n$ where n = 1 and 2 [47]. Kalläne et al [48] used photoelectron microspectroscopy to investigate the misfit layer compound (PbS)_{1,13}TaS₂. Their spectra show two components each for the Pb and Ta core levels. They conclude that there is a metal cross substitution of Ta atoms into the PbS layers and Pb atoms into the TaS2 layers that stabilizes the MLC. Photoelectron spectroscopy data from the ferecrystal heterostructures presented here show clear evidence for interlayer charge transfer without signs of a metal cross substitution (section 3).

A deeper understanding of the interactions between the individual layers is crucial, if one wants to systematically control the properties of these newly designed materials. The results presented here are the first direct investigation of the electronic structure of ferecrystals using XPS. (PbSe)_{1+ δ} (NbSe₂)₂ and (SnSe)_{1+ δ} (NbSe₂)₂ ferecrystals were investigated. Ferecrystals with m=1 and n=2 were chosen to keep the systems and results relatively simple. The binding energies of the Pb (or Sn), Nb and Se core levels were measured and compared to those of the respective binary bulk compounds PbSe, SnSe and NbSe₂. If a charge transfer takes place, it should be directly visible in a change in core level binding energy. In addition, valence band spectra were taken and modeled as a superposition of the bulk constituents.

2. Experimental details

(PbSe)_{1+ δ}(NbSe₂)₂ and (SnSe)_{1+ δ}(NbSe₂)₂ ferecrystals as well as PbSe, SnSe and NbSe₂ binary bulk compounds were synthesized from amorphous, modulated precursors via the modulated elemental reactants (MER) technique developed by Johnson and co-workers [49, 50]. To form the targeted compound with specific m and n values, a multi-layered precursor with calibrated layer thicknesses is prepared via sequential physical vapor deposition of amorphous elemental M, T and X layers [51]. The crystalline compound then self-assembles upon low-temperature annealing in N₂ atmosphere. The necessary calibration procedure for this process has been described in detail by Atkins *et al* [52].

The precursors were evaporated onto Si(100) substrates from high-purity metal sources in a custom-built vacuum chamber at a base pressure of about 1×10^{-8} mbar. A LabView program was used to position the substrates over each elemental source and the amount of evaporated material was controlled using a pneumatic shutter. Elemental Pb, Sn, Nb and Se layers were repeatedly deposited to mimic the appearance of the target compound. This was repeated until a total film thickness of about 50 nm was reached. After deposition, the precursors were transferred into a glovebox and annealed in an N2 atmosphere with less than 0.5 ppm O2 to induce crystallization. Annealing times for the samples used in this work ranged from 20 min to 60 min at 350-400 °C depending on composition. The formed compounds have a layered structure that is crystallographically aligned with the substrate, but adjacent layers show a randomly rotated orientation which is typical for products from the MER synthesis. The schematic structure of a (MSe)_{1+ δ}(NbSe₂)₂ ferecrystal is depicted in figures 1(a) and (c). Previously published [33] results obtained from a Rietfield refinement on x-ray diffraction data on the $(SnSe)_{1+\delta}(NbSe_2)_2$ compound is shown exemplarily in figure 3. The thickness of the indivual layers was determined in previous studies to be 0.612 nm for PbSe. 0.588 nm for SnSe and 0.630 nm and 0.635 nm for NbSe2 in $[(PbSe)_{1+\delta}]_m(NbSe_2)_n$ and $[(SnSe)_{1+\delta}]_m(NbSe_2)_n$ ferecrystals, respectively [32, 33]. Crystallite size is on the order of ≤15 nm, and adjacent grains show rotational disorder even within the same layer [19]. As a detailed discussion of the structural properties would go beyond the scope of this manuscript, we kindly refer the interested reader to the extensive studies on the preparation and structure on a wide range of $[(PbSe)_{1+\delta}]_m(NbSe_2)_n$ and $[(SnSe)_{1+\delta}]_m(NbSe_2)_n$ ferecrystals published elsewhere [32–36].

XPS measurements were carried out at room temperature in a UHV chamber at a pressure of approximately 3×10^{-10} mbar. Excitation of the photoelectrons was done using monochromated Al K_{α} radiation provided by a SPECS XR50M x-ray source equipped with a SPECS FOCUS 500 crystal monochromator. A SPECS Phoibos 150 MCD-9 hemispherical analyzer with nine channeltrons was used for analysis and detection of the photoelectrons. For the XPS measurements carried out in normal emission (0°) detection geometry of the photoelectrons, the x-ray source was oriented at an angle of about 45° relative to the crystal's c-axis. Binding energies are

referenced to the Au4f core level at 84.0 eV. The total energy resolution of the experiments shown is better than approximately 350 meV. The uncertainties of the core level binding energies is estimated to be 50 meV. Clean surfaces were prepared by cleaving. To that end, the samples were mounted onto the sample holders using a silver-filled, low degassing EPO-TEK H22 epoxy adhesive. The same epoxy was used to glue a steel plate on top of the sample, which was broken off in the load lock of the system under dry N₂ flow. The sample was rapidly transferred into UHV, where XPS survey spectra showed that the freshly cleaved surface was free of contaminants such as oxygen or carbon.

3. Results and discussion

XPS core level spectra were obtained for both binary bulk compounds as well as ferecrystals. First, we will discuss the Pb and Sn core levels for PbSe and $(PbSe)_{1+\delta}(NbSe_2)_2$, and SnSe and $(SnSe)_{1+\delta}(NbSe_2)_2$, respectively. As both Sn and Pb are group 14 elements, we would expect a similar behavior of the electronic structures in both ferecrystals. Following this, the Nb and Se core levels as well as valence band spectra are discussed. An overview of the binding energies obtained from peak analysis is given in figure 8.

The Pb5d doublet is shown in figure 4(a) for both the binary compound PbSe and the ferecrystal (PbSe)_{1+δ} (NbSe₂)₂. The Pb5d core level was used for peak analysis, because the more intense Pb4f spectrum interferes with the intense L₂M₄₅M₄₅ Auger transition of selenium. Since PbSe is a narrow bandgap semiconductor [53], the peak form is symmetric in the binary compound and the data can be fitted using a doublet of Voigt lines separated by a spin-orbit splitting of 2.60 eV. The branching ratio is 0.69, which is close to the theoretical value of 0.67 for a d-level [54]. A Shirley background was used for the fits [55]. The obtained binding energy of 18.84 eV for the Pb5d_{5/2} peak is consistent with previous results on (polycrystalline) PbSe [56]. In the spectrum of (PbSe)_{1+δ}(NbSe₂)₂, distinct differences to the spectrum of PbSe are observed. The Pb5d core level shifts by 0.47 eV towards lower binding energy compared to binary PbSe. In addition, the peaks show a slight asymmetry towards higher binding energy in the ferecrystal. A fit with an asymmetric function as derived by Mahan [57] gives a binding energy of 18.37 eV, an asymmetry parameter of $\alpha = 0.11$ and a cut-off energy of $\eta = 0.40$ eV. Note that for a Mahan fit, the binding energy is not where the peak maximum is. The asymmetry in the spectra of the PbSe layers, along with the shift in binding energy, indicates that charge transfer takes place from PbSe to NbSe₂. We attribute this to electrons being donated from the PbSe layer into the NbSe2 layer. By donating electrons into the NbSe₂ layers, the Fermi energy E_F of PbSe is shifted from within the band gap to inside the Se4p band (see figure 2), thus lowering the binding energy of the core levels. This is consistent with the results obtained by Alemayehu et al from analyzing transport properties of $[(PbSe)_{1+\delta}]_m(NbSe_2)_n$ ferecrystals [32]. The occurrence of a metal cross substitution

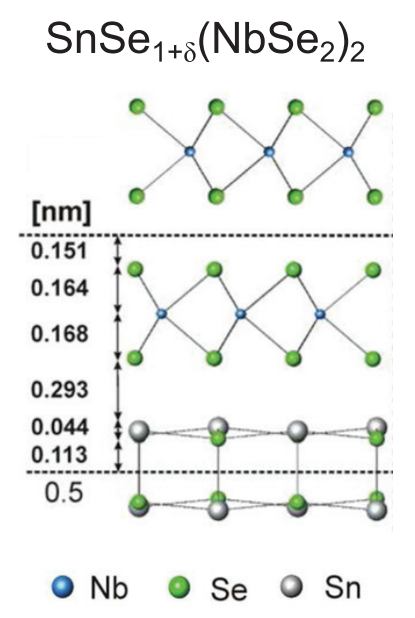


Figure 3. Structural parameters of $(SnSe)_{1+\delta}(NbSe_2)_2$ as a result of Rietfield refinements from x-ray diffraction data. The atomic positions along the c-axis of the crystal are shown. The mirror planes of the assigned P-3m1 space group are depicted with dotted lines. Reprinted with permission from [33]. Copyright 2015 American Chemical Society.

can be ruled out because only a single component contributes to spectrum of the ferecrystal.

As can be seen from the Sn3d core level spectra for SnSe and $(SnSe)_{1+\delta}(NbSe_2)_2$ in figure 4(b), we can observe trends of the peak shapes and core level binding energies in $(SnSe)_{1+\delta}(NbSe_2)_2$ similar to $(PbSe)_{1+\delta}(NbSe_2)_2$. Like PbSe, the binary compound SnSe is a semiconductor [58] and thus, the data can be fitted using a doublet of symmetric Voigt lines with a spin-orbit splitting of 8.41 eV and a branching ratio of 0.70. The binding energy of the $3d_{5/2}$ peak is at 485.87 eV, which is in good agreement with the values reported for cleaved single crystals of SnSe [56]. In the ferecrystal, a larger asymmetry with $\alpha = 0.45$ and $\eta = 0.64$ eV can be observed and the binding energy is 485.30 eV. The peak thus shifts by 0.57 eV towards lower binding energies. Using the same rationale as above, this can be explained by the SnSe layers donating electrons into the NbSe₂ layers. Again, the results are consistent with the charge transfer deduced from the transport measurements by Alemayehu et al [33, 34] As the Sn3d spectrum consists of only a single component in the ferecrystal, we conclude that there is no metal cross substitution present.

It should be noted that SnSe is known to undergo a size induced phase transition when the thickness is decreased from bulk to few layers of SnSe [16, 17, 59, 60]. In the bulk, the rocksalt layers have an orthorombic structure. With decreasing layer thickness, there is a continuous transition to a pseudote-tragonal structure. This behavior is similar to the phase transition observed in SnSe crystals at 807 K [61]. The effect of this phase transition on the electronic structure of ferecrystals has yet to be explored. However, both phases are semiconducting

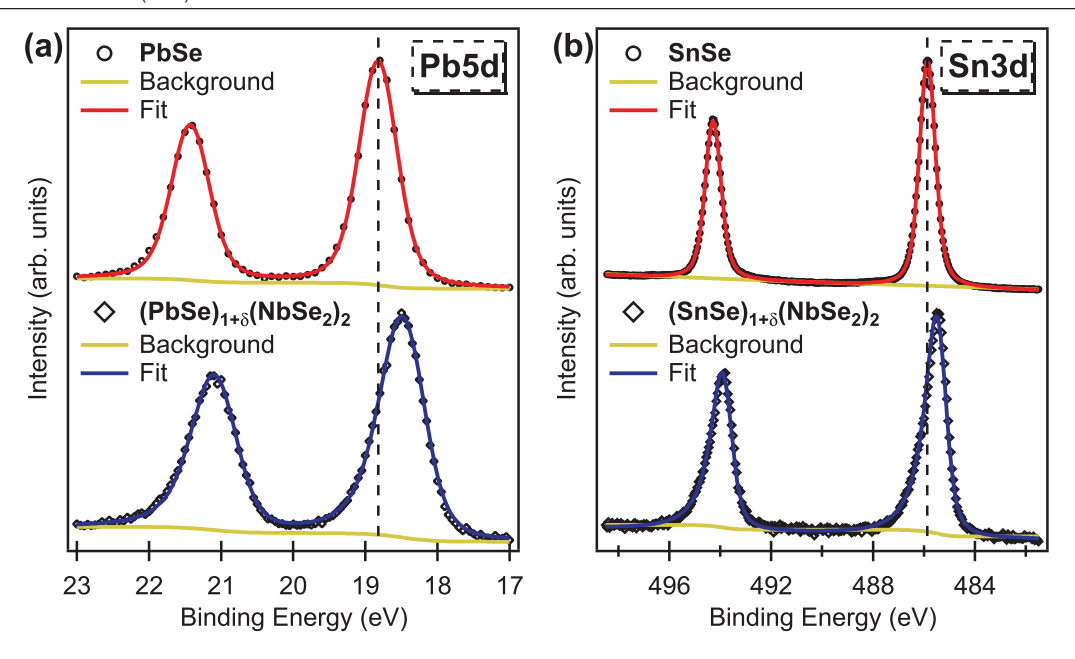


Figure 4. Comparison of the core level spectra of the metal atoms in the MSe layers of binary bulk crystals PbSe and SnSe (top row) and ferecrystals (PbSe) $_{1+\delta}$ (NbSe $_{2}$) $_{2}$ and (SnSe) $_{1+\delta}$ (NbSe $_{2}$) $_{2}$ (bottom row): (a) Pb5d, (b) Sn3d. For both compounds, a shift to lower binding energies and an asymmetric peak shape can be observed in the ferecrystals.

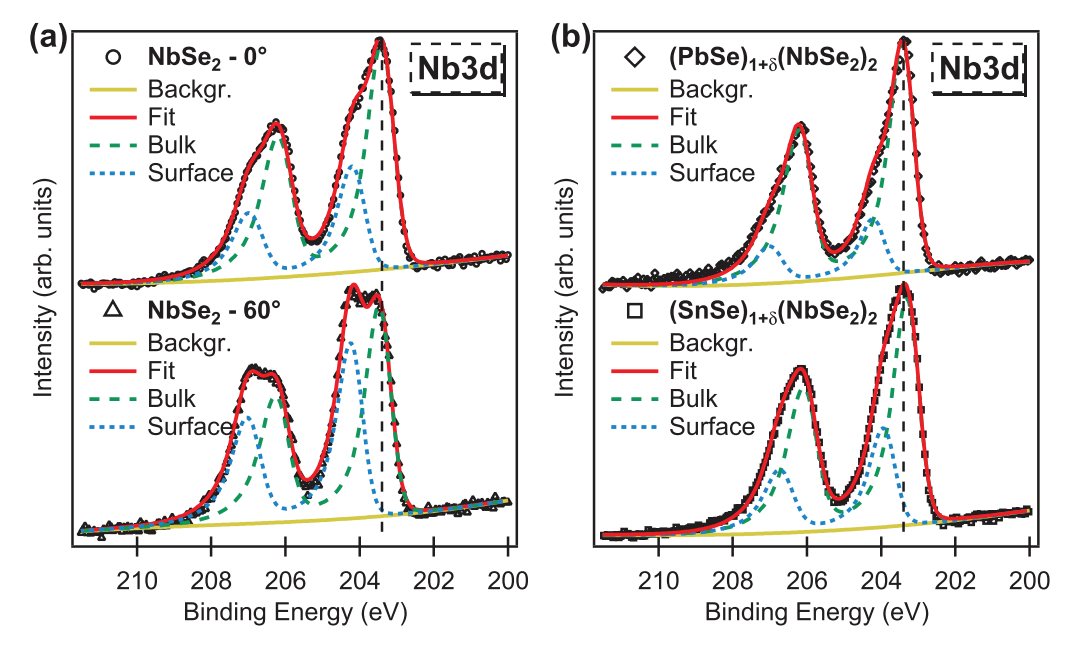


Figure 5. (a) Comparison of the Nb3d core level spectra of binary NbSe₂ in normal emission and at a detection angle of 60° . Two components are needed to fit the spectra, with the one at higher binding energies being more pronounced in the geometry with higher surface sensitivity. (b) Nb3d core level spectra of the ferecrystals (PbSe)_{1+ δ}(NbSe₂)₂ and (SnSe)_{1+ δ}(NbSe₂)₂. See text for more information.

[62]. We thus conclude that the observed asymmetry and the shift of the binding energy of the Sn3d core level are primarily caused by electron transfer.

In figure 5(a) the Nb3d core level spectra are shown for bulk NbSe₂. The normal emission spectrum (top, 0°) shows the presence of a shoulder at the higher binding energy side of the peak, which points to a second component in the spectrum. From measurements carried out under different detection angles, we could confirm that this second component is

a surface effect, as its relative intensity is increased when a more surface sensitive detection geometry is used (bottom, 60°). Peak analysis is not straightforward, as the background is influenced by the tail of the very intense selenium $L_3M_{45}M_{45}$ Auger transition at 178 eV. Thus, the background was approximated by a polynomial curve. The peak shape assigned to the bulk is asymmetric, as NbSe₂ is a p-type metal at room temperature [63]. The spectrum was fitted using two doublets of Mahan lines, with identical lifetime and Gaussian widths,

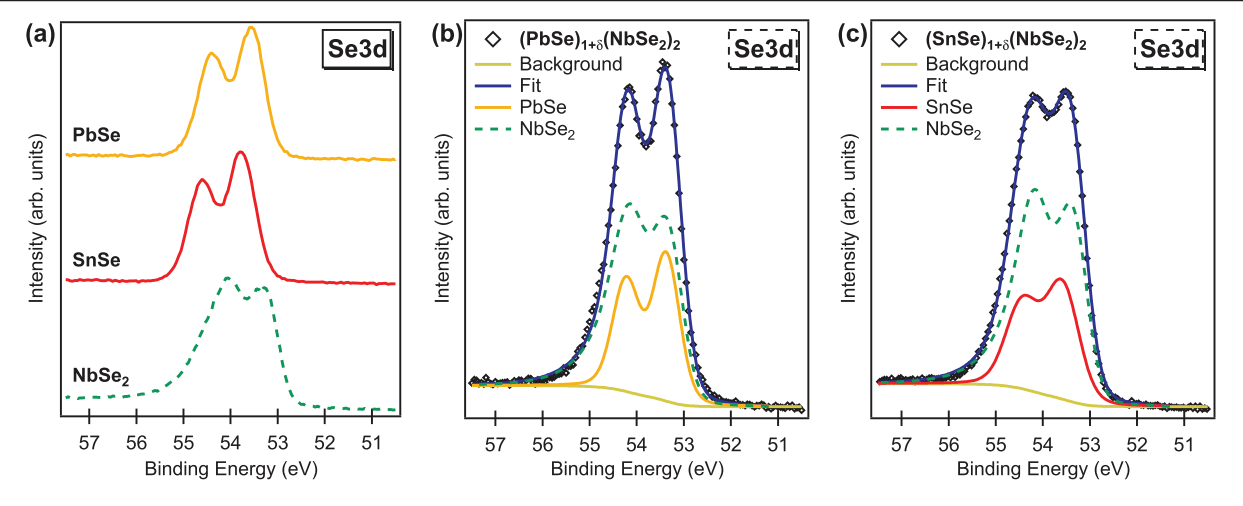


Figure 6. (a) Se3d core level spectra of the binary compounds PbSe, SnSe and NbSe₂. ((b) and (c)): Se3d core level spectra of (PbSe)_{1+ δ} (NbSe₂)₂ and (SnSe)_{1+ δ} (NbSe₂)₂ ferecrystals, fitted as a superposition of the binary compounds PbSe, SnSe and NbSe₂, respectively.

asymmetry parameter α and cut-off energy η . α and η were determined from best fits to be 0.4 and 0.83 eV, respectively. Chiang et~al~[64] report a higher cut-off energy for NbSe₂ single crystals, but they do not discuss a surface component. The binding energy of the bulk material (green) is 203.18 eV and the shift of the surface component (blue) is 0.77 eV. Surface oxidation can be ruled out as the origin of the surface component, because XPS survey scans show no oxygen. It might be due to the termination of the bulk material, but this is still an open question and part of ongoing investigations.

In the ferecrystals (figure 5(b)), the overall peak shape appears to be similar to the binary compound. The surface component, which is clearly visible in the binary, is also present but much less pronounced, especially for the (PbSe)_{1+ δ} (NbSe₂)₂ ferecrystals. The shift of 0.66 eV for this second component is slightly smaller in $(SnSe)_{1+\delta}(NbSe_2)_2$ than that of $0.87 \,\mathrm{eV}$ in $(\mathrm{PbSe})_{1+\delta}(\mathrm{NbSe}_2)_2$. As the ferecrystals are also metals with holes as the majority charge carriers [32–34, 36], the peak shape is asymmetric as well. The binding energy of the main component stays the same within experimental uncertainty (see figure 8). We therefore conclude that the electronic structure of the NbSe2 layers is conserved in the ferecrystals and shows no shift. The absence of a shift of the electronic structure of the NbSe₂ layers can be explained by the high density of states of the about half-filled Nb4d band at the Fermi level (see also figure 2). It can accept charges without significantly changing the electronic structure of the NbSe₂ layers and the Fermi energy.

The Se3d core level spectra of the three binary compounds PbSe, SnSe and NbSe₂ are shown in figure 6(a). The binding energy of the Se3d_{5/2} was determined from fits to be 53.54 eV in PbSe, 53.77 eV in SnSe and 53.11 eV in NbSe₂, while the spin-orbit splitting amounts to about 0.85 eV (0.85 eV in PbSe, 0.85 eV in SnSe, 0.84 eV in NbSe₂). The observed branching ratio is larger than the theoretical expectation of 0.67 for a d-level for all three compounds (0.77 in PbSe, 0.75 in SnSe and 0.80 in NbSe₂). This is due to a resonant process described in detail by Wertheim *et al* [65, 66]. Due to the metallic nature

of bulk NbSe₂, the doublet shows an asymmetric tail towards higher binding energy.

Figures 6(b) and (c) show the measured Se3d spectra (data points) for representative $(PbSe)_{1+\delta}(NbSe_2)_2$ and $(SnSe)_{1+\delta}(NbSe_2)_2$ ferecrystals, respectively. The spectrum of the ferecrystal was fitted as a weighted superposition of the spectra of the bulk binary compounds PbSe (or SnSe) and NbSe₂. To reduce the number of free parameters, the asymmetry parameter, cut-off energy, branching ratio and lifetime width of the respective doublet peaks were constrained to the values obtained from the binary compounds. Only a shift in binding energy and a Gaussian broadening of the doublets was allowed. As can be seen from figure 8, the component we assigned to PbSe shifts 0.23 eV towards lower binding energy in $(PbSe)_{1+\delta}(NbSe_2)_2$ while the $NbSe_2$ -component does not shift. The same trend can be observed for $(SnSe)_{1+\delta}(NbSe_2)_2$, where the component assigned to SnSe shifts by 0.20eV towards lower binding energies and the NbSe2 component stays at a constant energy within experimental uncertainty. This is consistent with the observed shift of the Pb and Sn core levels and the absence thereof in the Nb3d core level. The relative intensities of the two components are about 70% NbSe₂ and 30% PbSe in (PbSe)_{1+ δ}(NbSe₂)₂, and about 58% NbSe₂ and 42% SnSe in (SnSe)_{1+ δ}(NbSe₂)₂ (averaged over multiple samples). The varying ratio of MSe to NbSe₂ from different samples is likely due to the cleave of the crystal occurring between different layers.

In addition to the core levels we measured valence band spectra of the binary compounds (PbSe, SnSe and NbSe₂) and the ferecrystals. They are shown in figure 7. Due to its metallic nature, the spectrum of NbSe₂ shows a clear Fermi edge at zero binding energy. In contrast to that, the spectra of the semiconducting PbSe and SnSe show no intensity at the Fermi energy. The valence band maxima of PbSe and SnSe were determined to be located at 0.45 eV and 0.37 eV, respectively.

In the framework of a rigid band model, the valence band density of states is usually regarded as a simple superposition of the respective binary compounds in the misfit layered

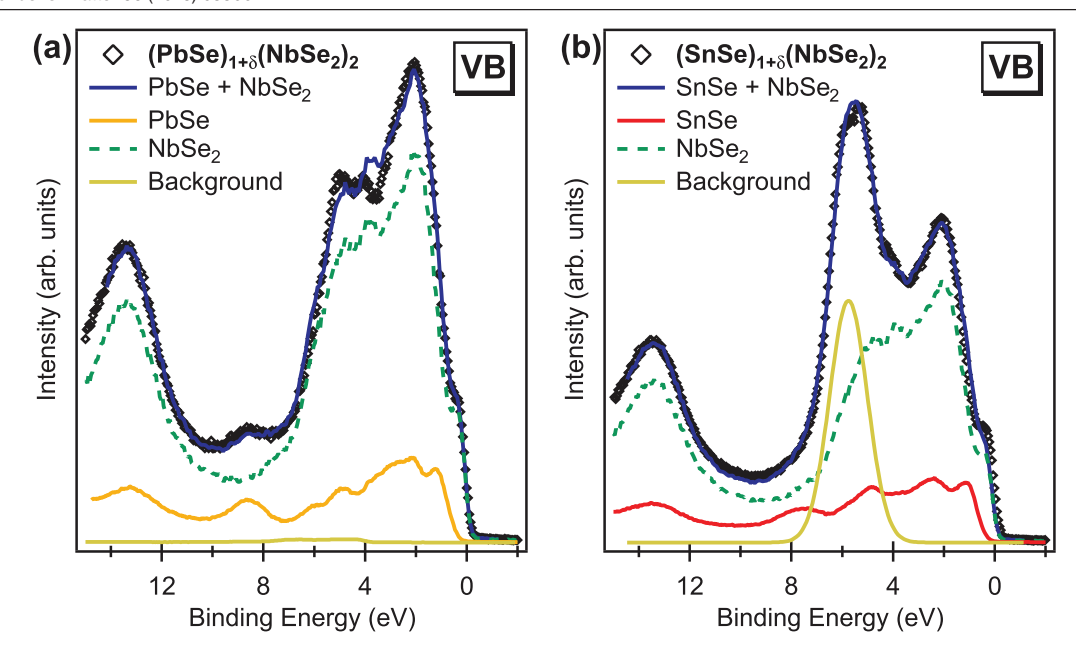


Figure 7. XPS valence band spectra of representative (a) $(PbSe)_{1+\delta}(NbSe_2)_2$ and (b) $(SnSe)_{1+\delta}(NbSe_2)_2$ ferecrystal samples (data points) measured with Al K_{α} radiation. The spectra are fitted as a superposition of the spectra of the binary compounds PbSe (or SnSe) and NbSe₂, which are shown shifted from their bulk position.

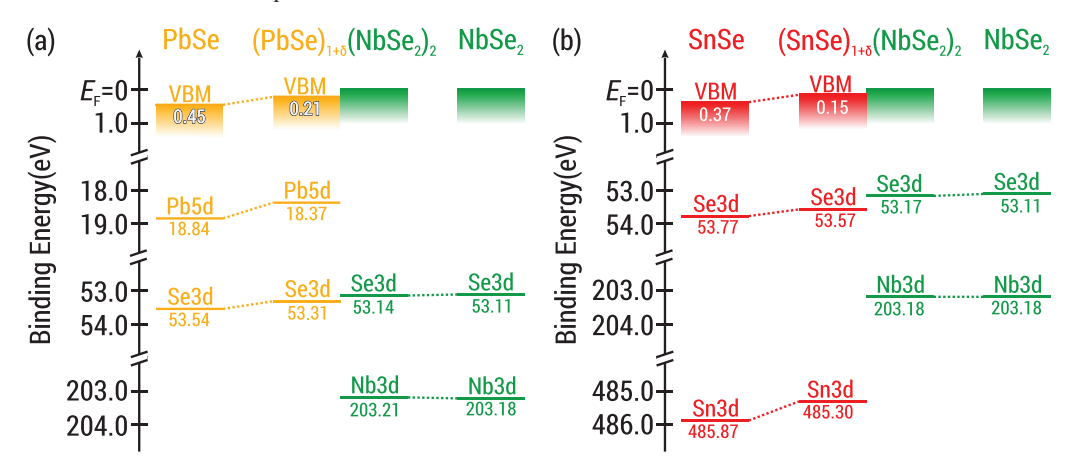


Figure 8. Energy diagram of the experimental binding energy shifts of core levels and valence band maximum (VBM) of (a) (PbSe)_{1+ δ} (NbSe₂)₂ and (b) (SnSe)_{1+ δ} (NbSe₂)₂ ferecrystals compared to the binary compounds PbSe, SnSe and NbSe₂.

compounds [41, 43, 47]. We used the same approach for our ferecrystals as shown in figure 7: the measured spectrum of the ferecrystal (data points) was fitted by a weighted superposition of the spectra of the two respective binary compounds. Additionally, the spectra of the binary compounds were free to shift in binding energy during the fit routine.

For $(PbSe)_{1+\delta}(NbSe_2)_2$, the data points are fairly well represented by a superposition of PbSe and NbSe₂ (figure 7(a)). The contribution of the PbSe layers is shifted by 0.24 eV towards lower binding energy, while the contribution of the NbSe₂ layers does not shift. This is consistent with the observed binding energy shifts of the core level analysis. Different peaks in the valence band spectrum can be assigned to Se4s around 13.5 eV and Pb6s around 8.9 eV. The broad band below the Fermi level is built up from the Se4p and the Nb4d band, which intersects the Fermi level.

In the case of $(SnSe)_{1+\delta}(NbSe_2)_2$ (figure 7(b)), the spectrum of the ferecrystal is disturbed by a large background peak centered around 6 eV. This stems from the silver filled epoxy adhesive used during the cleaving process (for the $(PbSe)_{1+\delta}(NbSe_2)_2$ samples, this background intensity is negligible). The contributions to the spectrum from the silver are due to holes in the film, that expose the underlying epoxy adhesive. This was confirmed by optical microscopy. In the modeling of the $(SnSe)_{1+\delta}(NbSe_2)_2$ valence band, treating this background as a single Voigt line worked well. Note that no silver core levels interfered with the shown core level spectra of the ferecrystals. The SnSe contribution has to be shifted towards lower binding energy by $0.22\,\mathrm{eV}$, while the NbSe₂ contribution does not shift, to model the spectrum.

Summarizing the experimental results, we see a shift of the core level and valence band spectra of the PbSe and SnSe layers towards lower binding energies in the ferecrystals. The experimentally observed changes in binding energy are shown in an energy diagram in figure 8. For PbSe, the Pb5d core level shifts by 0.47 eV, the Se3d core level by 0.23 eV and the valence band by 0.24 eV. The Sn3d core level of SnSe shifts by 0.57 eV, Se3d by 0.20 eV and the valence band by 0.22 eV. The observed trend is consistent for all core levels and the valence band.

The observed shifts of the metal core levels are larger than that for selenium. This is probably due to some necessary simplifications made during the deconvolution of the Se3d spectrum, as the two components assigned to MSe and NbSe2 are in close proximity to each other. Since the peak shape of the metal core levels becomes asymmetric in the ferecrystals, we would assume the same to also happen to the MSe component of the Se core levels. Using the asymmetric Mahan line shape for the MSe component during deconvolution would likely compensate for the observed difference in binding energy shift, but was omitted to reduce the number of free parameters. For the valence band a simple model of a weighted superposition was used. The observed shift is in agreement with the core level shifts within the limits of the resolution. The core level and valence band spectra of the NbSe2 layers show no shift in the ferecrystal compared to the binary compound. The experimental observations are consistent with the conclusions from transport measurements [32-34], that the MSe layers donate electrons into the charge accepting NbSe₂ layers. As the area analyzed by XPS is large compared to the crystal's grain size, the obtained spectra are integrated over all possible rotation angles between randomly orientated layers. The observed peak widths in the binary compounds and the ferecrystals are similar, and thus we conclude that the amount of charge transferred between layers is independent of the rotation angle between adjacent layers within the resolution of the instrument. Since the spectra show no additional components in the ferecrystals, we conclude that there is no cross substitution of metal atoms between the layers.

4. Conclusions

We investigated layered ferecrystal heterostructures (PbSe) $_{1+\delta}$ (NbSe2) $_2$ and (SnSe) $_{1+\delta}$ (NbSe2) $_2$ using x-ray photoelectron spectroscopy. The core levels of Pb, Sn, Se and Nb were compared to the respective binary compounds PbSe, SnSe and NbSe2. Analysis of the core level spectra showed a shift of the electronic structure of PbSe and SnSe towards lower binding energy in the ferecrystal when compared to the bulk material, while the electronic structure of the NbSe2 layers is conserved and shows no shift. We could thus confirm that the PbSe and SnSe layers donate electrons into the NbSe2 layers, which can accept charges without changing the electronic structure due to the high density of states at the Fermi level in the Nb4d band. This is further supported by an asymmetry observed in the Pb and Sn core levels of the ferecrystals.

Within a rigid band model, the valence band of the ferecrystals can be approximated by a weighted superposition of the valence bands of the respective binary components. The contributions from the PbSe and SnSe layers shift towards lower binding energy, while that from NbSe₂ layers shows no shift. This is consistent with the observations from the core level spectra. Our data do not show any signs of a metal cross substitution, which was suggested to occur in some misfit layered compounds, presumably resulting from the high temperatures and long annealing times used in their synthesis. The observed charge transfer between constituents provides opportunities to modulation dope one layer via charge transfer from another. The charge transfer, combined with the ability to change the identity, thickness and alloy the rock salt constituent provides opportunities to continuously tune the Fermi level to optimize physical properties.

ORCID iDs

Fabian Göhler https://orcid.org/0000-0003-2299-2445 Gavin Mitchson https://orcid.org/0000-0002-0840-2376

References

- [1] Novoselov K S, Geim A K, Morozov S V, Jiang D, Zhang Y, Dubonos S V, Grigorieva I V and Firsov A A 2004 Science 306 666
- [2] Sutter P, Huang Y and Sutter E 2014 Nano Lett. 14 4846
- [3] Geim A K and Grigorieva I V 2013 Nature 499 419
- [4] Chhowalla M, Shin H S, Eda G, Li L J, Loh K P and Zhang H 2013 Nat. Chem. 5 263
- [5] Ferrari A C et al 2015 Nanoscale 7 4598
- [6] Kuc A, Heine T and Kis A 2015 MRS Bull. 40 577
- [7] Kaul A B 2014 J. Mater. Res. 29 348
- [8] Novoselov K S, Fal'ko V I, Colombo L, Gellert P R, Schwab M G and Kim K 2012 Nature 490 192
- [9] Mannix A J et al 2015 Science 350 1513
- [10] Mayorov A S et al 2011 Nano Lett. 11 2396
- [11] Wang L et al 2013 Science 342 614
- [12] Ni G X et al 2015 Nat. Mater. 14 1217
- [13] Miyata Y, Nakayama K, Sugawara K, Sato T and Takahashi T 2015 Nat. Mater. 14 775
- [14] Alemayehu M B, Falmbigl M, Ta K, Ditto J, Medlin D L and Johnson D C 2015 Angew. Chem. 127 15688
- [15] Anderson M D, Heideman C L, Lin Q, Smeller M, Kokenyesi R, Herzing A A, Anderson I M, Keszler D A, Zschack P and Johnson D C 2013 Angew. Chem. Int. Ed. 52 1982
- [16] Beekman M, Disch S, Rouvimov S, Kasinathan D, Koepernik K, Rosner H, Zschack P, Neumann W S and Johnson D C 2013 Angew. Chem. Int. Ed. 52 13211
- [17] Falmbigl M, Alemayehu M B, Merrill D R, Beekman M and Johnson D C 2015 Cryst. Res. Technol. 50 464
- [18] Beekman M, Heideman C L and Johnson D C 2014 Semicond. Sci. Technol. 29 064012
- [19] Alemayehu M B, Falmbigl M, Grosse C, Ta K, Fischer S F and Johnson D C 2015 J. Alloys Compd. 619 861
- [20] Wiegers G 1996 Prog. Solid State Chem. 24 1
- [21] Rouxel J, Meerschaut A and Wiegers G 1995 J. Alloys Compd. 229 144
- [22] Moore D B, Beekman M, Disch S and Johnson D C 2014 Angew. Chem. 126 5778
- [23] Heideman C L, Rostek R, Anderson M D, Herzing A A, Anderson I M and Johnson D C 2010 J. Electron. Mater. 39 1476

- [24] Lin Q, Smeller M, Heideman C L, Zschack P, Koyano M, Anderson M D, Kykyneshi R, Keszler D A, Anderson I M and Johnson D C 2010 Chem. Mater. 22 1002
- [25] Heideman C L, Tepfer S, Lin Q, Rostek R, Zschack P, Anderson M D, Anderson I M and Johnson D C 2013 J. Am. Chem. Soc. 135 11055
- [26] Esters M, Alemayehu M B, Jones Z, Nguyen N T, Anderson M D, Grosse C, Fischer S F and Johnson D C 2014 Angew. Chem. Int. Ed. 54 1130
- [27] Atkins R, Moore D B and Johnson D C 2013 Chem. Mater. 25 1744
- [28] Merrill D, Moore D, Bauers S, Falmbigl M and Johnson D 2015 Materials 8 2000
- [29] Moore D B, Beekman M, Disch S, Zschack P, Häusler I, Neumann W and Johnson D C 2013 Chem. Mater. 25 2404
- [30] Merrill D R, Moore D B, Coffey M N, Jansons A W, Falmbigl M and Johnson D C 2014 Semicond. Sci. Technol. 29 064004
- [31] Merrill D R, Sutherland D R, Ditto J, Bauers S R, Falmbigl M, Medlin D L and Johnson D C 2015 Chem. Mater. 27 4066
- [32] Alemayehu M B, Mitchson G, Hanken B E, Asta M and Johnson D C 2014 *Chem. Mater.* **26** 1859
- [33] Alemayehu M B, Falmbigl M, Ta K and Johnson D C 2015 Chem. Mater. 27 2158
- [34] Alemayehu M B, Ta K, Falmbigl M and Johnson D C 2015 Nanoscale 7 7378
- [35] Alemayehu M B, Ta K, Falmbigl M and Johnson D C 2015 J. Am. Chem. Soc. 137 4831
- [36] Alemayehu M B, Falmbigl M, Ta K, Grosse C, Westover R D, Bauers S R, Fischer S F and Johnson D C 2015 Chem. Mater. 27 867
- [37] Alemayehu M B, Falmbigl M, Ta K and Johnson D C 2015 ACS Nano 9 4427
- [38] Wiegers G 1995 J. Alloys Compd. 219 152
- [39] Ettema A R H F, Haas C and Turner T S 1993 Phys. Rev. B 47 12794
- [40] Ettema A R H F and Haas C 1993 J. Phys.: Condens. Matter 5 3817
- [41] Ohno Y 1991 Phys. Rev. B 44 1281
- [42] Ohno Y 1991 Solid State Commun. 79 1081
- [43] Fang C, Ettema A, Haas C, Wiegers G, van Leuken H and de Groot R 1995 Phys. Rev. B 52 2336

- [44] Moëlo Y, Meerschaut A, Rouxel J and Auriel C 1995 Chem. Mater. 7 1759
- [45] Meerschaut A, Moëlo Y, Cario L, Lafond A and Deudon C 2000 Mol. Cryst. Liq. Cryst. 341 1
- [46] Brandt J et al 2001 J. Electron Spectrosc. Relat. Phenom. 114-116 555
- [47] Brandt J, Kipp L, Skibowski M, Krasovskii E, Schattke W, Spiecker E, Dieker C and Jäger W 2003 Surf. Sci. 532 705
- [48] Kalläne M, Roßnagel K, Marczynski-Bühlow M, Kipp L, Starnberg H I and Stoltz S E 2008 Phys. Rev. Lett. 100 065502
- [49] Johnson D C 1998 Curr. Opin. Solid State Mater. Sci. 3 159
- [50] Noh M, Johnson C D, Hornbostel M D, Thiel J and Johnson D C 1996 Chem. Mater. 8 1625
- [51] Heideman C, Nyugen N, Hanni J, Lin Q, Duncombe S, Johnson D C and Zschack P 2008 J. Solid State Chem. 181 1701
- [52] Atkins R, Wilson J, Zschack P, Grosse C, Neumann W and Johnson D C 2012 Chem. Mater. 24 4594
- [53] Dalven R 1969 Infrared Phys. 9 141
- [54] Briggs D and Seah M (ed) 1990 Practical Surface Analysis. Auger and X-Ray Photoelectron Spectroscopy vol 1, 2nd edn (Chichester: Wiley)
- [55] Shirley D A 1972 Phys. Rev. B 5 4709
- [56] Shalvoy R B, Fisher G B and Stiles P J 1977 Phys. Rev. B 15 1680
- [57] Mahan G D 1975 Phys. Rev. B 11 4814
- [58] Yu J, Yue A and Stafsudd O 1981 J. Cryst. Growth 54 248
- [59] Ludemann M, Gordan O D, Zahn D R, Beekman M, Atkins R and Johnson D C 2014 Langmuir 30 8209
- [60] Beekman M, Disch S, Gunning N and Johnson D C 2015 Inorg. Chem. 54 1091
- [61] Wiedemeier H and Csillag F J 1979 Z. Kristallogr.—Cryst. Mater. 149 17
- [62] Shi G and Kioupakis E 2015 J. Appl. Phys. 117 065103
- [63] Lee H N S, McKinzie H, Tannhauser D S and Wold A 1969 J. Appl. Phys. 40 602
- [64] Chiang S, Wertheim G and DiSalvo F 1976 Solid State Commun. 19 75
- [65] Wertheim G, DiSalvo F and Buchanan D 1983 Phys. Rev. B 28 3335
- [66] Wertheim G 1984 J. Electron Spectrosc. Relat. Phenom. 33 79